HHS Public Access

Author manuscript

Nat Chem Biol. Author manuscript; available in PMC 2020 February 21.

Published in final edited form as:

Nat Chem Biol. 2019 December ; 15(12): 1165–1172. doi:10.1038/s41589-018-0176-3.

A DNA-based fluorescent reporter maps HOCl production in the maturing phagosome

Shareefa Thekkan[1,2], **Maulik S. Jani**[1,2], **Chang Cui**[3,4], **Krishna Dan**[1,2], **Guolin Zhou**[4], **Lev Becker**[*,3,4], **Yamuna Krishnan**[*,1,2]

[1]Department of Chemistry, The University of Chicago, Chicago, Illinois 60637, USA.

[2]Grossman Institute of Neuroscience, Quantitative Biology and Human Behavior, The University of Chicago, Chicago, Illinois 60637, USA.

[3]Committee on Cancer Biology, Ben May Department for Cancer Research, The University of Chicago, Chicago, IL 60637, USA.

[4]Ben May Department for Cancer Research, The University of Chicago, Chicago, IL 60637, USA.

Abstract

Phagocytes destroy pathogens by trapping them in a transient organelle called the phagosome where they are bombarded with reactive oxygen (ROS) and reactive nitrogen species (RNS). Imaging reactive species within the phagosome would directly reveal the chemical dynamics underlying pathogen destruction. Here we introduce a fluorescent, DNA-based combination reporter, cHOClate which simultaneously images HOCl and pH quantitatively. Using cHOClate targeted to phagosomes in live cells we successfully map phagosomal production of a specific ROS i.e. hypochlorous acid (HOCl), as a function of phagosome maturation. We found that phagosomal acidification was gradual in macrophages and upon completion, HOCl was released in a burst. This revealed that phagosome-lysosome fusion was essential not only for phagosome acidification, but also to provide the chloride necessary for myeloperoxidase activity. This method can be expanded to image several kinds of ROS and RNS and be readily applied to identify how resistant pathogens evade phagosomal killing.

Introduction

The immune system comprises phagocytes whose main function is to destroy pathogens by engulfing and trapping them in a sub-cellular organelle called the phagosome[1]. The

*Correspondence to: yamuna@uchicago.edu and levb@uchicago.edu.

Author contributions

S.T. and Y.K. designed the project. S.T. and K.D performed chemical synthesis. S.T synthesized and characterized the sensor. C.C. and G.Z isolated and characterized primary cells from human and mice. M.S.J. contributed immunostaining and western blot expertise. S.T and M.J performed imaging experiments. S.T., M.S.J., L.B. and Y.K. analyzed the data. S.T. and Y.K. wrote the paper. All authors discussed the results and gave inputs on the manuscript.

Competing financial interests

The authors declare no competing financial interests.

Data availability

The data that support the plots within this paper and other finding of this study are available from the corresponding authors upon reasonable request.

phagosomal milieu is rapidly transformed into a toxic hotspot brought about by the highly localized production of reactive oxygen species (ROS) and reactive nitrogen species (RNS) that participate in pathogen killing[2,3]. Other organelles such as lysosomes assist this process by fusing with the phagosome and thereby delivering payloads of destructive enzymes into the phagosomal milieu[4]. Once the pathogen is cleared, the phagosome disappears. A technology capable of chemically mapping the evolution of reactive species during the maturation of a transient organelle like the phagosome will offer new insights into the actual production of pathogen destruction as a function of the host and the pathogen. Since resistant microbes use several mechanisms to avoid phagosomal degradation, such a technology would offer insight into how resistant pathogens by-pass phagosomal killing[5]. Here, using a DNA-based, pH-independent, ratiometric fluorescent reporter that is targeted to phagosomes, we chemically map the phagosomal production of a specific ROS i.e., hypochlorous acid (HOCl) in real time and as a function of phagosome maturation in live cells.

One such destructive enzyme delivered to the phagosome is myeloperoxidase (MPO)[6]. MPO is a lysosome-resident, heme protein that produces a powerful reactive species – hypochlorous acid (HOCl) - using both hydrogen peroxide (H_2O_2) and chloride as its substrates[6,7]. MPO is the only known producer of HOCl, so measuring HOCl is a specific and direct readout of MPO activity. HOCl exists in equilibrium with hypochlorite anion ($HOCl/OCl^-$, pKa 7.53) in the cellular environment. It is one of the most effective microbicidal agents of any host cell, a frontline defender in innate immunity and is secreted copiously by neutrophils when they are activated. However, when dysregulated, MPO activity leads to deleterious effects in immune-mediated inflammatory diseases including multiple sclerosis, acute coronary syndrome, renal disease, atherosclerosis and organ damage[8]. MPO is active when it is either secreted extracellularly or upon its delivery to the phagosome since it requires both H_2O_2 as well as a chloride-rich environment[7,8]. While phagosomal MPO is highly beneficial due to the effective containment of HOCl within the host cell, secreted MPO is thought to be responsible for its deleterious effects[8,9]. Despite the existence of several methods to quantitate extracellular MPO activity, mapping phagosomal MPO activity has proved elusive[10–12]. Therefore, the ability to selectively map phagosomal HOCl would enable the identification of new regulators of MPO secretion that could have therapeutic value in immune-mediated inflammatory diseases.

There is still no protein-based reporter that has been targeted to the phagosome, to image HOCl specifically. Several excellent detection chemistries for ROS, RNS and specifically HOCl based on small molecules exist, but the reacted probe molecules diffuse rapidly, blurring out spatial information[13–18]. DNA nanostructures have enabled the quantitative imaging of physiologically relevant ions or small molecules in organelles of living cells in culture and *in vivo*[19–24]. DNA-based reporters combine the advantages of small molecule probes with the stable localization provided by biological macromolecules. The modular nature of the DNA scaffold enables one to leverage the 1:1 stoichiometry of DNA hybridization to simultaneously integrate multiple functions with stoichiometric precision onto a single probe. Thus, we have realized a DNA-based reporter that can simultaneously and quantitatively map HOCl and pH in the phagosome by integrating (i) an HOCl sensitive fluorophore (ii) a pH sensitive fluorophore - both, functions accessible to small molecule

probes (iii) an internal standard for simultaneous ratiometric quantitation of both HOCl & pH and (iv) a phagosome targeting function for stable sub-cellular localization.

Using this phagosome targetable sensor called Z-cHOClate we could map the pH and HOCl changes in innate immune cells such as macrophages, neutrophils and monocytes and give a comparison of MPO activity in these cells. The high sensitivity of Z-cHOClate to HOCl reveals that mouse macrophages have do have MPO, not reported previously due to its low levels of activity in these cells.

Results

A ratiometric, pH-independent reporter of MPO activity

First, we describe the design, creation and characterization of a pH-independent, DNA-based, ratiometric, fluorescent reporter of HOCl, and therefore MPO activity, called cHOClate (Fig.1a). We identified a molecule whose fluorescence was sensitive to HOCl. We found that the water-soluble and photostable Cyanine dye 1,1′-bis(3-sulfopropyl)-3,3,3′,3′-tetramethyl-5,5’-disulfo-indodicarbocyanine (**1**), (red star, λ_{ex} = 650 nm; λ_{em} = 665 nm) underwent oxidative cleavage specifically with HOCl thereby losing its fluorescence[25]. Cyanine dye derivatives are prone to cleavage by HOCl[15–17], and in comparison with other reports, (**1**) shows relatively lower sensitivity which proved advantageous for subsequent applications[26,27]. Mass spectrometry revealed that (**1**) was oxidatively cleaved to 1-(3-sulfopropyl)-3,3-dimethyl-5-sulfo-oxindole (**2**) and 1-(3-sulfopropyl)-2-(5-oxo-pent-1,3-dienyl)-3,3-dimethyl-5-Sulfo-indole (**3**) (Fig. 1b), thus functioning as a turn-off sensor for HOCl in the concentration regime of 5 μM – 1 mM (Supplementary Fig. 1a and 1b).

cHOClate is a 50-base pair DNA duplex comprising three strands I, II and III (Supplementary Table 1 for sequences) and bears four functionalities of which two will be discussed now and two later (Fig. 1a and 2a). The first of these is a HOCl sensing dye (red star, R), (**1**) at the 3’ end of strand I (red strand). The second is a reference dye Atto-488 (blue oval, λ_{ex} = 488 nm; λ_{em}=520 nm) attached to the 3’end of strand II (blue strand, Fig. 1a and 2a). Atto-488 was used as a reference fluorophore because of its high photostability and insensitivity to pH, ROS and RNS. The formation and integrity of cHOClate was confirmed using gel electrophoresis and fluorescence spectroscopy that indicated >99% yield (Supplementary Fig. 2 and 3, Supplementary table 2).

The concentration of solution HOCl is reflected in the ratio (R/B) of the fluorescence intensities of Atto-488 (B) and (**1**) (R) (Supplementary Fig. 4a) in cHOClate. To test this, varying concentrations of NaOCl (0–100 μM) were added to cHOClate (100 nM) in UB_4 buffer (20 mM, at pH 4.5), and fluorescence emission of both Atto-488 and (**1**) were recorded as a function of time. While the fluorescence of Atto-488 remained unchanged, the fluorescence of (**1**) reduced as a function of increasing HOCl (Fig. 1c) over the reported physiological HOCl concentrations (20–400 μM)[28]. The response time for 80% signal change was < 2 minutes for 40 μM HOCl, indicating a fast response (Fig. 1e). Importantly, the R/B ratio of cHOClate remained constant over a range of solution pH indicating that the sensitivity of cHOClate to HOCl was pH-independent from pH 7 to pH 4.5 (Supplementary Fig. 5).

Next, the specificity of cHOClate towards various reactive oxygen species (ROS) or reactive nitrogen species (RNS) was tested by incubating it with generators of specific reactive species for 10 minutes and subsequently measuring R/B values. cHOClate showed ~20-fold selectivity for HOCl over any other ROS/RNS (Fig. 1d and Supplementary Fig. 4b). Note that on longer timescales i.e., 20 minutes, we observed very modest sensitivity to peroxynitrite ($ONOO^-$) (Supplementary Fig. 4c). Additionally, we checked the stability of the DNA scaffold to reactive species and found that over the time-scales studied, the duplex integrity was quantitatively maintained (Supplementary Fig. 6 and 7). The rapid response, pH insensitivity, good specificity to HOCl and stability of the DNA scaffold positions cHOClate very well to quantitatively image phagosomal HOCl over the short timescales of phagosome maturation.

cHOClate simultaneously detects pH and HOCl

Upon phagocytosis, the phagosome undergoes maturation that is characterized by progressive acidification in macrophages while it remains near neutral in neutrophils[29]. In order to map HOCl in the phagosome as a function of phagosome maturation, we designed cHOClate such that it could simultaneously report pH and HOCl. Thus, cHOClate incorporates a third functionality namely, the dye N-(6-Aminohexyl) rhodamine 6G-amide (R6G, λ_{ex} = 530 nm; λ_{em} = 555 nm) which undergoes acid mediated lactam ring opening, sensing pH reversibly (Supplementary Fig. 8)[30]. R6G (green diamond, Fig. 2a) shows enhanced fluorescence at acidic pH and is attached to the 3’ end of a 26-mer DNA strand III (Fig. 2a and Supplementary Fig. 9, green strand). The fourth functionality is a conjugation module in the form of a Dibenzocyclooctyl group (DBCO) at the 5’-end of strand I (Fig. 2a) in order to conjugate cHOClate to a phagocytic cargo through azidealkyne click chemistry.

cHOClate functioned well as a ratiometric reporter of solution pH. The ratio of R6G fluorescence (G) to Atto-488 fluorescence (B) in cHOClate i.e., G/B ratio, quantitatively reports pH where G/B increases as acidity increases. cHOClate showed a 10-fold increase in G/B from pH 7.4 (extracellular pH) to ~pH 5 (lumenal pH in a mature phagosome)[29] (Fig. 2b and c), indicating that it was also well placed to report on phagosomal pH. Just as the R/B ratio remains unaffected at all investigated pH values, the G/B ratio remains unaffected from 0 – 100 μM HOCl (Supplementary Fig. 4d). Thus, the pH sensing module is insensitive to HOCl levels.

Next, in order to target cHOClate to the phagosome we sought to conjugate it to zymosan particles that are a well-documented phagocytic cargo[31]. Zymosan is a cell wall preparation of heat-inactivated yeast, *S. Cerevisiae*. Because the surface of zymosan particles are rich in β−1,3- and β−1,6- Glucans, we could functionalize the surface of zymosan by periodate oxidation of β−1,6- Glucan[32]. This was immediately followed by condensation with the bifunctional linker NH_2-PEG_3-N_3 and *in situ* $NaBH_4$ reduction of the resultant Schiff’s base (Fig. 2d and Supplementary Fig.10). This resulted in zymosan particles being surface-modified to display azido groups (Zym-N_3), which could be subsequently conjugated with cHOClate by incubation for 4 h at RT. Excess cHOClate was removed by repeated washes in phosphate buffer (20 mM, pH 7.4). This procedure yielded surface labelling of ~98% of the particles as observed by FACS coated with ~10^6 molecules of cHOClate on average

(Supplementary Fig. 11–13 and online methods: Estimate of cHOClate molecules per zymosan). The response characteristics of Zym-N_3 covalently coated with cHOClate, called z-cHOClate, was then evaluated by fluorescence imaging at various concentrations of HOCl and solution pH.

First, the pH response of z-cHOClate was evaluated by incubation in solutions of different pH, followed by fluorescence imaging in the Alexa488, R6G and (**1**) channels. The ratio of R/B and G/B of n = 50 particles as a function of pH revealed 6-fold increase in G/B from extracellular pH (7.4) to mature phagosomal pH (4.5) while R/B remains unaffected (Fig. 2e, Supplementary Fig. 11b). Next, a similar experiment with increasing concentrations of HOCl from 0–20 μM revealed that R/B ratio underwent a 100-fold decrease, while the G/B ratio was unaffected (Supplementary Fig. 11c). Thus z-cHOClate is able to report on pH as well as HOCl such that neither sensing module interferes with the other and each module quantitatively retains its sensing characteristics.

cHOClate measures phagosomal HOCl production

First, we checked the performance of z-cHOClate to detect changes in lumenal pH and HOCl inside a phagosome using in-situ pH and HOCl clamping in J774A.1 cells. Z-cHOClate inside phagosomes senses changes in pH and HOCl levels with the same sensitivity as extracellular particles confirming that performance of z-cHOClate is not affected in side cells (Supplementary Fig. 14 and 15). We then examined the in-cell specificity of z-cHOClate to HOCl by pharmacologically inhibiting proteins that produce specific reactive species. We chose the murine macrophage cell line J774A.1 due to its well-described propensity to phagocytose a variety of micron-sized particles, especially zymosan[33–35]. Cells were incubated with z-cHOClate for 5 minutes, and then imaged every 3 minutes for 30 minutes post-phagocytosis. J774A.1 cells phagocytosed z-cHOClate as efficiently as zymosan indicating that cHOClate coating did not significantly perturb phagocytosis. Since previous reports provided evidence for phagosome maturation in macrophages and MPO activity in neutrophils well within 20 minutes post phagocytosis, we limited our investigations to under 30 minutes post phagocytosis[18,29].

We then measured the HOCl levels given by the R/B ratio of phagocytosed z-cHOClate in mature phagosomes as the latter are easily identified by their G/B value. MPO produces HOCl using both H_2O_2 and Cl^- as substrates. The former is derived due to the activity of NOX2 and the latter is derived from phagosome-resident channels and transporters, or when the chloride-rich lysosome fuses with the phagosome[34,36].

In mature phagosomes of J774A.1 cells treated with 200 nM 1400W which is a specific inhibitor of iNOS, we observed that both R/B and G/B values were similar to those of untreated cells (Fig. 3a–b). This revealed that reactive nitrogen species such as NO were not responsible for the photophysical changes undergone by z-cHOClate in the phagosome. Upon treatment with 20 μM DPI, a NOX2 inhibitor or 100 μM ABAH, an MPO inhibitor, the G/B value in the phagosome was similar to untreated cells, indicating that the phagosome acidified normally (Fig. 3a – b). However, the R/B value was comparable to uninternalized z-cHOClate (Fig. 3b), indicating that the reactive species resulting from NOX2 activity or MPO activity were the entities being sensed by z-cHOClate. In order to

confirm that z-cHOClate reports on HOCl as a result of MPO activity, we also treated cells with increasing amounts of NPPB, a pan chloride channel blocker, expected to decrease lumenal Cl^- levels in all endocytic organelles including the phagosome[37]. Accordingly, we found that although phagosomal acidification occurred normally as revealed by the G/B ratio, the R/B ratio showed a dose-dependent increase, confirming specific detection of HOCl due to MPO activity within the phagosome (Fig. 3a and c).

Next, we sought to map phagosomal HOCl production in concert with phagosomal acidification using z-cHOClate in live cells. Figure 3d shows the pseudocolor maps of G/B (upper panel) and R/B (lower panel) values of J774A.1 cells that have just phagocytosed z-cHOClate. The G/B ratio progresses from lower values (blue) to higher values (red) in line with phagosomal acidification. On the other hand, in the same phagosome, the R/B ratio progresses from higher values (red) to lower values (blue) indicating a progressive increase of HOCl within the phagosome (Fig. 3d–e). The phagosome acidifies rapidly from 5 minutes onwards, reaching maximum acidity at ~12 minutes post internalization (Fig. 3d; Supplementary movies 1 and 2). The maximum fold change in G/B observed for phagocytosed z-cHOClate revealed that the pH of mature phagosomes in J774A.1 cells was pH 6.0 (Fig. 3b and Supplementary Fig. 14). This is in very good agreement with other studies of phagosomal pH in macrophages[38].

Phagosomal HOCl, on the other hand, developed very slowly over the first ~8 minutes, reflected in the slow decrease in R/B signal, and, after a critical level of acidification was reached, there was a burst of HOCl reflected by a sharp decay in the R/B ratio that occurred over 3 minutes (t = 12–15 minutes) (Fig. 3d–e). Cells treated with ABAH showed normal acidification of phagosome and no change in the R/B signal over this duration (Supplementary Fig. 16a and Supplementary movies 3 and 4) reaffirming that z-cHOClate indeed reported on HOCl production. Further, R/B and G/B values of extracellular z-cHOClate particles remain unaffected during the time course of the experiment, revealing that any signal change due to photobleaching is negligible in the time window investigated (Fig. 3e). We could similarly map phagosomal HOCl in other mouse macrophage cell lines like RAW264.7 and SIM-A9 (Supplementary Fig. 16b–c).

Myeloperoxidase comprises nearly 5% of total protein in neutrophils. We similarly mapped phagosomal pH and HOCl kinetics in human neutrophils. In order to enhance phagosome labeling in neutrophils, we opsonized z-cHOClate using human IgG. While phagosomal pH in neutrophils remained near neutral, we observed a burst of HOCl 5–10 minutes post phagocytosis (Supplementary Fig. S17). Comparing the percentage signal change due to HOCl production in neutrophils, monocytes and monocyte derived macrophages (HMDMs) after 20 minutes of phagocytosis, we find that neutrophils have the highest level of myeloperoxidase (MPO) activity in the phagosome, next monocytes and finally, macrophages (Supplementary Fig. S18). This correlates well with MPO levels found in neutrophils, monocytes and macrophages estimated by us and others[39].

Phagocytosis upregulates MPO in macrophages

Inflammatory diseases such as multiple sclerosis and atherosclerosis are characterized both by high MPO levels as well as an abundance of activated macrophages[8]. To date, MPO in

these contexts is considered to be largely derived from neutrophils and the role of macrophage-derived MPO has not yet been addressed. This is because of the comparatively lower quantities of HOCl produced by macrophages as well as the lack of a suitable reporter technology for intracellular MPO.

Human macrophages produce HOCl upon immunostimulation. However, because of the diffusible nature of both HOCl and its existing reporters it remains unclear whether this HOCl is produced by secreted or phagosomal MPO[13,18]. We investigated this using two approaches. First, we pulsed control and activated human monocyte derived macrophages (HMDMs) with *z-cHOCate* and measured phagosomal MPO activity (Fig. 4a). We found that phagosomal HOCl levels increased, following LPS stimulation (Fig. 4a) and this increase could be abolished by ABAH inhibition of MPO. Second, control and LPS-activated HMDMs were pulsed with R6G-Zym and immunostained for MPO (Fig. 4b). Interestingly HMDMs showed only a marginal increase in MPO levels when treated with LPS compared to untreated cells (Fig. 4b). However, within 30 minutes post-phagocytosis, activated HMDMs substantially upregulated MPO and immunostaining revealed that most of it was phagosomal (Fig. 4b–c).

Previous studies on mouse macrophages have suggested that HOCl levels have been too low to detect due to poor MPO expression in these cells[40,41]. However, given our findings that both activation and phagocytosis could cause MPO upregulation, we performed a similar experiment with mouse bone marrow derived macrophages (BMDMs). By immunofluorescence, we found that activated BMDMs showed increased levels of MPO within the phagosome (Fig. 4d and e). This difference in MPO levels was reflected in the HOCl levels, as detected using z-cHOClate (Supplementary Fig. S16c). A similar result was obtained in J774A.1 cells (Supplementary Fig. S19a – b) that was also confirmed by Western blot for MPO (Supplementary Fig. S19c). Together, this revealed that phagocytosis of zymosan by immunostimulated macrophages upregulates intracellular MPO, which roughly doubles the production of HOCl in the phagosome. Further, BMDMs derived from wild type mice ($MPO^{+/+}$) showed a large decrease (60%) in R/B signal, while those derived from $MPO^{-/-}$ showed negligible decrease (<5%) in R/B signal compared to uninternalized particles indicating that z-cHOClate is a highly sensitive and specific reporter of phagosomal HOCl (Fig. 4f).

Given the ability of z-cHOClate to sensitively map phagosomal HOCl, we then explored the capacity of primary murine macrophages from different tissue sources to produce phagosomal HOCl. Phagosomes in primary tissue macrophages derived from mouse adipose (ATM) and peritoneum (PM) labeled with z-cHOClate showed a 4-fold and 2-fold change respectively in the R/B ratio (Fig. 4f). Mouse macrophages have long been considered insignificant producers of HOCl based largely on measurements of extracellular HOCl. However, this direct observation of endogenous, intracellular HOCl in primary mouse tissue macrophages reveals that they are in fact effective at producing phagosomal HOCl.

Discussion

We have been able to map the production of a reactive species within the phagosome as a function of phagosome maturation using a phagosome-targeted, DNA-based combination reporter. Because lumenal acidity is one of the major functional indicators of phagosome maturation, it necessitated the simultaneous measurement of phagosomal acidity as well as the reactive species of interest. The intrinsic modularity of the DNA scaffold allows one to integrate ratiometric sensor modules for two different analytes, such that both analytes can be sensed simultaneously and independently of each other. cHOClate leverages the modular nature of DNA to integrate ratiometric pH and HOCl sensors such that they function independently to provide information on pH and HOCl levels at the same time, at the same location.

The modularity of DNA was further utilized to integrate a conjugation center on cHOClate such that we could covalently attach it to the surface of zymosan particles. This enabled us to target cHOClate exclusively to the phagosome where it mapped the evolution of pH and HOCl simultaneously during phagosome maturation. Our studies revealed that phagosomal acidification was a gradual, continuous process in macrophages, that was initiated 3–4 minutes post-phagocytosis and needed ~10 minutes for maturation. On the other hand, HOCl production showed a distinct burst upon the phagosome reaching its maximal acidity. Such a reactive species burst has been predicted by measures of extracellular ROS and NO, as well as of total ROS in neutrophil phagosomes, albeit without the temporal information associated with maturation[42–44].

Our studies reveal that in addition to acidifying the phagosome as well as delivering MPO, lysosome fusion likely elevates phagosomal chloride to the levels needed to efficiently produce HOCl. NPPB treatment reveals no alteration either in uptake or acidification within phagosomes. Given that the response of (**1**) to HOCl is pH-independent, this rules out that the burst is simply due to protonation of ClO^- to HOCl due to a sudden pH drop. Further, the reaction of HOCl with (**1**) is slower than protonation, therefore we can reliably conclude that the sharp drop in R/B ratio is due to a surge in MPO activity. Recent studies support this conclusion where, defective pathogen clearance was observed in mouse macrophages lacking CLCN7, a CLC channel that mediates lysosomal chloride accumulation without affecting lysosomal pH[45]. Taken together this suggests a role for lysosomal chloride in innate immunity, where it drives phagosomal MPO activity for pathogen degradation.

Our studies have identified macrophages as a potential additional cellular source of MPO that could be involved in pathophysiology. For example, atherosclerotic plaques are characterized by an abundance of chlorinated products due to MPO activity[8]. Though circulating neutrophils have been considered the main source of MPO, activated macrophages are the most abundant in atheroma and our new technology shows that activated murine and human macrophages can generate phagosomal HOCl via MPO. Although it is tempting to speculate that macrophages may also be a source of MPO activity in the atherosclerotic lesion, further investigations are needed to address this prediction.

Most ROS or RNS probes with high selectivity and sensitivity are based on irreversible, stoichiometric reactions[46]. The standard assumptions for such reactive species probes is that they consume only a small fraction of the total reactive species generated in order to report analyte levels, and that the probes preferentially react with the reactive species of interest compared to the generic, non-specific cleavage they cause the phagocytosed cargo. Since Z-cHOClate is an irreversible reporter of HOCl, it must first be calibrated within the desired host cell before quantitating HOCl production rates.

MPO levels are lowered or increased due to immunosuppression or immune activation[47–49]. We can therefore envisage phenotypic cellular assays for immunosuppression or immune activation in immune cells derived directly from blood draws using cHOClate. We can also obtain single cell level information on immune activation since the cHOClate probes are retained in immune cells. Utilizing cHOClate one can identify new small molecule inhibitors or activators of MPO. Finally, this methodology can be extended to map many other reactive species such as H_2O_2, superoxide, nitric oxide etc. for which excellent fluorescent detection chemistries already exist[46,50–52]. It can be extended to map the phagosomal milieu for different kinds of surface-labeled pathogens that enter the cell through phagocytosis. This would enable the study of early-stage host-pathogen interaction production and the most effective chemical means of pathogen clearance within the phagosome especially for pathogens like *S. aureus* and *M. tuberculosis* that evade the immune response[5].

Online Methods

Materials.

All oligonucleotides (Supplementary Table 1) were purchased from IDT (USA). HPLC purified DNA oligonucleotides were used without further purification, whereas fluorescently modified oligonucleotides were ethanol precipitated prior to further use. Strand III was functionalized as shown in Supplementary Fig. 3a. Oligos were quantified using UV-Vis spectrophotometry (Shimadzu UV-2700), dissolved in Milli-Q water to prepare a 200 μM stock, and aliquoted and stored at −20°C.

1400W and DEA-NONOate were purchased from Cayman chemicals. All other chemicals were purchased from Sigma Aldrich. Unlabeled Zymosan was purchased from Thermo Fisher scientific. Stock solutions of 1400W, DPI, ABAH and NPPB at 50 mM were prepared in DMSO (50 mM). Stock solutions of ROS generators were prepared in MQ water (5mM), except DEA-NONOate which was prepared in NaOH (10 mM, pH 9), and were all used within a week.

1,1′-bis(3-sulfopropyl)-3,3,3′,3′-tetramethyl-5,5’-disulfo-indodicarbocyanine (1) as a HOCl reporter:

The nature of the reaction between **1** and HOCl was verified using a carboxylic acid derivative of **1.** Briefly 50 μM of **1** was treated with 1 mM of HOCl and stirred for 15 minutes at room temperature. The resulting mixture was subjected to LC MS on an Advion Expression-L mass spectrometer (Ithaca, NY). Mass spectrometry revealed the oxidized products of **1** on reaction with HOCl. The reaction was further confirmed by UV

spectrophotometry. For this 1 μM of **1** was treated with 0–300 μM of HOCl at pH 7 (phosphate buffer, 10 mM) for 10 minutes and UV spectra was recorded for each sample from 400 nm – 750 nm, a gradual decrease in the absorbance of was observed (Supplementary Fig. 1b).

Functionalizing III with R6G.

The pH-sensing module was prepared by reaction between azide functionalized strand III with R6G-DBCO (**5**). First, **5** was synthesized as described by supplementary scheme 1. 200 μM of **5** was added to a solution of Strand-III-N_3 (50 μM) in 50 mM potassium phosphate buffer, pH 7 and stirred overnight at RT. The resultant product was ethanol precipitated and characterized using gel electrophoresis (Supplementary Fig. 9).

Assembly and characterization of cHOClate

Strands I, II and III were mixed in equimolar ratios to a final concentration of 20 μM in 20 mM potassium phosphate buffer, pH 7 containing 100 mM KCl. Annealing was performed by heating to 90 °C for 5 minutes, cooling to room temperature over 3 hr at 5°C/15 min and equilibrating at 4°C overnight. Prior to conjugation, the solution was diluted to 10 μM in 20 mM potassium phosphate buffer, pH 7 containing 100 mM KCl.

Formation of cHOClate was confirmed by a gel mobility shift assay using 10% native PAGE. The gel was imaged using *BIO-RAD* ChemiDoc MP imaging system for fluorophores. The gel was further stained with EtBr solution for 5 minutes and imaged in EtBr channel. There is a bleed through for Atto-488 in Epi-green filter set, as observed in the gel due to lack of appropriate filters in the instrument (Supplementary Fig. 2).

In vitro fluorescence measurements

All fluorescence studies were carried out on a Fluoromax-4 (Horiba Scientific, Edison, NJ, USA) spectrophotometer. For fluorescence experiments 100 nM of cHOClate was used. Fluorescence from Atto-488 (Blue, λ_{ex} = 488 nm, λ_{em} = 520 nm), R6G (Green, λ_{ex} = 530 nm, λ_{em} = 555 nm) or **1**(Red, λ_{ex} = 650 nm, λ_{em} = 665 nm) was recorded with excitation and emission slit widths of 3 nm. All fluorescence experiments were done in 20 mM UB_4 buffer (20mM HEPES, 20mM MES, and 20mM sodium acetate) at 37°C at the indicated pH unless otherwise stated. R/B represents the ratio of emission intensities of **1** to Atto-488 (665 nm/520 nm) and G/B represents the ratio of emission intensities of R6G to Atto-488 (555 nm/520 nm). All spectra were blank corrected and normalized to the intensity of cHOClate without ROS/RNS at the respective pH.

HOCl sensitivity and kinetics

Solutions of 100 nM cHOClate in 20 mM UB_4, pH 4.5, were incubated with NaOCl (0 to 100 μM) for 10 minutes at 37°C. Fluorescent emission spectra were recorded in red, green, and blue channels corresponding to 665 nm (R), 555 nm (G) and 520 nm (B) respectively, blank corrected and normalized to no added NaOCl.

To check pH dependence of cHOClate to HOCl, 100nM of cHOClate was incubated with HOCl ranging from 1 nM −100 μM at various values of pH from pH 7.0 – 5.0 (UB_4 buffer,

100 mM). R/B values and G/B values of cHOClate were measured at t = 20 min post addition of HOCl.

For kinetic studies, 100 nM cHOClate was added to a cuvette at pH 4.5 and 37°C and initial R/B was measured. To this, 40 μM NaOCl was added and spectra were taken in red and blue channels at 1, 2, 5, 10, 15, 20 minutes. The ratio of R/B at each time point was normalized to R/B before HOCl addition and plotted against time.

In vitro specificity experiments

Aqueous NaOCl served as a HOCl donor where OCl^- concentration was quantified using ε = 350 $M^{-1}cm^{-1}$ at 292 nm. Aqueous H_2O_2 served as a H_2O_2 donor where its concentration was quantified using ε =43.6 $M^{-1}cm^{-1}$ at 240 nm. Peroxynitrite was prepared *in situ* from $NaNO_2$ and H_2O_2 as reported and quantified using ε =1670 $M^{-1}cm^{-1}$ at 302 nm[53]. Xanthine/Xanthine oxidase was used to generate superoxide, which was quantified using Cytochrome C reduction as described[54]. Fenton chemistry was used for the generation of hydroxyl radical (·OH) and tert-Butyl peroxide radical (·TBH)[54]. DEA-NONOate was used as a NO donor.

ROS/RNS generators were added to 100 nM of cHOClate in 20 mM UB4, pH 4.5, to a final concentration of 100 μM reactive species, except for HOCl, in which 40 μM NaOCl was added. Samples were incubated for 10 minutes at 37°C and fluorescence spectra were recorded in all channels. Fold change of R/B in each case was normalized to that of cHOClate without ROS/RNS.

pH sensitivity for cHOClate

cHOClate was incubated in 20 mM UB_4 buffer, pH 4.5–7.5, for 5 minutes at 37°C and fluorescence spectra were recorded in red (λ_{ex} = 650 nm), blue (λ_{ex} = 488 nm) and green (λ_{ex} = 530 nm) channels as mentioned earlier. Ratios of R/B and G/B were plotted against pH.

Surface functionalization of Zymosan to Z-cHOClate

1 mg of Zymosan (2×10^7 particles) was stirred with 0.34 mg of $NaIO_4$ (2 nmol) in 80 μL of 50 mM sodium acetate buffer, pH 5, at 4°C in the dark for 16 h to oxidize 1,6-glucans on the surface. To quench unreacted $NaIO_4$, 4 μL ethylene glycol was added, stirred for 10 minutes, and centrifuged at 2500 rpm for 15 minutes at 4°C. Supernatant was removed without disturbing the pellet and replaced 100 μM of NH_2-PEG-N_3 in 100 mM borate buffer, pH 10. After stirring for 24h at RT in the dark, the supernatant was removed by centrifugation, and the Schiff base formed was stabilized by $NaBH_4$ (3 nmol) in Milli-Q water. This azide-functionalized Zymosan (Zym-N_3) was incubated with cHOClate (10 μM) in 20 mM phosphate buffer, pH 7 with 100 mM KCl, for 4h at RT in the dark. The resulting suspension was centrifuged, washed the pellet with 1x PBS (*3 times) and resuspended in potassium phosphate buffer of pH 7(20mM containing 100 mM KCl). Surface labeling was evaluated by imaging particles at pH 5. As a control for surface labeling, unfunctionalized zymosan particles were treated with cHOClate and imaged (Supplementary Fig. 11a).

Surface functionalization of Zymosan to R6G-Zym

1 mg of Zymosan (2×10^7 particles) was stirred with 0.34 mg of $NaIO_4$ (2 nmol) in 80 μL of 50 mM sodium acetate buffer, pH 5, at 4°C in the dark for 16 h to oxidize 1,6-glucans on the surface. To quench unreacted $NaIO_4$, 4 μL ethylene glycol was added, stirred for 10 minutes, and centrifuged at 2500 rpm for 15 minutes at 4°C. Supernatant was removed without disturbing the pellet and replaced with N-(6-Aminohexyl) rhodamine 6G-amide bis(trifluoroacetate)(R6G) (1.3 μmol) in 100 mM borate buffer, pH 10 containing 20% DMSO. After stirring for 24h at RT in the dark, the supernatant was removed by centrifugation, and the Schiff base formed was stabilized by $NaBH_4$ (3 nmol) in MQ water. The R6G-functionalized Zymosan (R6G-Zym) was characterized by fluorescent imaging and used for immunostaining experiments.

Estimate of cHOClate molecules per zymosan

Estimate from a small molecule-based cleavage assay: We synthesized the BCN-coumarin molecule (**8**) which was then chemically attached to the azide groups displayed on Zym-N_3(Supplementary scheme 2). This displays hydrolysable 7-hydroxy-4-trifluoromethylcoumarin groups (λ_{max} = 385 nm, ε= 20573 $M^{-1}cm^{-1}$) on the Zym- N_3 surface to give Zym-(**8**). Roughly 10^6 Zym-(**8**) particles were subjected to base hydrolysis of carbonate groups to release trifluoromethylcoumarin into a well-defined solution volume, which was then estimated by UV absorption (Supplementary Fig. 13). This yielded ~27.5×10^7smalle molecules per zymosan.

Briefly Zym-N_3 (1.7×10^6) was labelled with (**8**) (20 μM, 1000 pmoles) as described earlier for Z-cHOClate. Any free dye was removed by centrifugation and washes with 1x PBS (6 times), 150 mM of Tris base (pH 9.5) was added to ~10^6 Zym-(**8**) particles and the mixture was stirred for 15 h at 50°C. The resultant suspension was centrifuged at 4000 rpm for 15 minutes, the supernatant was collected. The particles were washed, all the supernatants collected (6×100 μL), combined, concentrated to 100 μL and quantified by UV absorption. Experiments were performed in duplicate.

$$\text{No of moles of cleaved coumarin} = 775 \pm 13 \text{ pmoles}$$

$$\text{No: of moles of azides for attachment / Zymosan} = 775 \pm 13 \text{ pmoles} / 1.7 \times 10^6$$

$$\text{Zymosan} = 456 \times 10^{-18} \text{ moles/Zymosan}$$

$$\text{No: of azide groups / Zymosan} = 6.023 * 10^{23} (456.5 \times 10^{-18}) = 27.5 \times 10^7$$

This corresponds to the maximum number of small molecules that can be displayed on Zym-N3. However, DNA is much larger than (**8**) and attachment at one site, might preclude accessibility to surrounding azides.

Theoretical estimate

Assuming Zymosan as a sphere and assuming 50% surface coverage, considering the charge repulsion between DNA duplexes that are radiating outwards from the Zym-N3 surface, we calculated the number of cHOClate molecules that can be accommodated on a zymosan particle.

Average diameter of a Zymosan particle $= 3.9\ \mu m$

Average surface area of a Zymosan $= 4\pi r^2 = 47.78\ \mu m^2$

50% surface area covered by DNA $= 47.78/2 = 23\ .89\ \mu m^2$

Radius of a DNA duplex ~ 1 nm

Area occupied by a vertically oriented DNA duplex $= \pi r^2 = 3.14\ nm^2$

Number of DNA molecules at 50% surface coverage $= 23890000\ nm^2/3.14\ nm^2 = 7.60\ \times\ 10^6$

Experimental estimate

Using UV absorbance, we measured the concentration of cHOClate in a solution that was used to functionalize ~10^6 Zym-N_3 particles before and after labeling. We were thus able to estimate the change in cHOClate concentration post labeling, which was then converted to the number of cHOClate molecules that was used up for labeling. Knowing the number of Zym-N_3 particles used for the reaction, the average number of cHOClate per Zym-N_3 particle was found to be ~3.87×10^6.

Both theoretical and experimental estimates are consistent with each other and are on the order of 10^6 DNA duplexes / zymosan particle.

pH sensitivity for Z-cHOClate

Z-cHOClate (4 μg/μL) was diluted 20-fold in UB_4 buffer, pH 4.5 – 7.5, and incubated for 5 minutes at 37 °C. Each solution was pipetted up and down 5 times and immediately transferred to a glass slide. The drop was covered with a 0.17 mm cover glass and incubated for 5 minutes to form a thin film. Glass slides were imaged in respective channels using an IX-83 microscope.

HOCl sensitivity of Z-cHOClate

Z-cHOClate (4 μg/μL) was diluted 20-fold in UB_4 buffer, pH 7 and incubated for 5 minutes with NaOCl (0 −20 μM) at 37°C. Each solution was pipetted up and down for 5 times, and immediately transferred to a glass slide. The drop was covered with a 0.17 mM cover glass and incubated for 5 minutes to form a thin film. Glass slides were imaged in respective channels using an IX-83 microscope and R/B and G/B in each case was calculated.

Cell culture

Mouse alveolar macrophage J774A.1 cells were a kind gift from Prof Deborah Nelson, Department of Pharmacological and Physiological Sciences, the University of Chicago. They were cultured in Dulbecco's Modified Eagle's Medium/F-12 (1:1) (DMEM-F12) (Invitrogen Corporation, USA) containing 10% heat inactivated Fetal Bovine Serum (FBS) (Invitrogen Corporation, USA) using ATCC protocols. RAW 264.7 cells were a kind gift from Dr. Christine A. Petersen, Department of Epidemiology, College of Public Health, University of Iowa. SIM-A9 (ATCC CRL-3265) cells were purchased from ATCC and cultured according to the ATCC protocol.

Primary cell culture

Human peripheral blood was obtained from healthy volunteers following obtaining a written consent in compliances with ethical regulations approved by the University of Chicago Institutional Review Board (IRB16–0321). Blood was collected in EDTA coated blood collection tubes, and Ficoll Paque Plus was used for separation. Monocytes were contained in the buffy coat layer, which was further isolated using anti-CD14 coupled magnetic beads and differentiated into human monocyte-derived macrophages by treating with M-CSF (125 ng/mL) in RPMI for 7 days as previously described[55] .Neutrophils were contained in the bottom layer and purified by repetitive RBC lysis steps. For LPS activation, differentiated macrophages were treated with 100 ng/mL LPS for 24 hours. Prior to pulse/chase experiments media was replaced with fresh RPMI.

Male C57BL/6 with $MPO^{+/+}$and $MPO^{-/-}$(JAX stock #004265) were purchased from Jackson laboratories. To prepare Bone Marrow Derived Macrophages (BMDMs), myeloid cells were isolated from femurs and tibia of WT and MPO KO mice as described[56]. Cells were differentiated to macrophages using murine M-CSF for 6 days. For LPS activation, cells were treated with 20 ng/mL LPS for 24 hours. Prior to pulse/chase experiments media was replaced with fresh RPMI. All animal studies are in compliances with ethical regulations approved by the University of Chicago Institutional Animal Care and Use Committee (ACUP 72209).

Mouse adipose tissue macrophages (ATM) were isolated from mammary tissue of WT mice as described[55]. Cells were counted using a hemocytometer, plated on glass bottom imaging dishes, and allowed to adhere for 2–3 hours prior to pulse/chase experiments.

To isolate peritoneal macrophages (PM), WT mice were injected with thioglycollate and cells were harvested from the peritoneal cavity 5 days after injection[57]. The cells were washed with phosphate-buffered saline (PBS), plated, and allowed to adhere to glass bottom imaging dishes at 37°C for 2 h in serum-free DMEM. Cells were then washed with PBS to remove non-adherent cells and used for pulse/chase experiments with Z-cHOClate.

Imaging experiments

For imaging experiments, J774A.1 and RAW 264.7 cells were scraped and plated in 35 mm glass bottom dishes and kept overnight at 37°C, 5% CO_2. SIM-A9 cells were detached using trypsin-EDTA and plated on 35 mm glass bottom dishes and kept overnight at 37°C, 5% CO_2. Seeded density of cells were 60%.

pH clamping in phagosome

J774A.1 cells were incubated with Z-cHOClate for 10-minutes in presence of 100 μM ABAH to allow for phagocytosis and cells were then fixed with 2.5% PFA. The cells were then incubated in a pH clamping buffers of a known pH values, say pH 4.5, using UB_4 buffer containing ionophores Nigericin (20 μM), Monensin (20 μM), 140 mM NaCl, 10 mM KCl, and 2.5 mM $CaCl_2$ for 30 minutes. Cells containing Z-cHOClate particles were imaged as described and the ratio of fluorescence intensities in green and blue channels (G/B) was obtained and compared with that of un-internalized Z-cHOClate particles as a control. The

experiment was performed for clamping buffers at different pH values spanning pH 4.5–7.5 and G/B values were plotted as a function of clamping buffer pH to obtain the calibration curve.

HOCl clamping in phagosome

J774A.1 cells plated on a glass bottom dish was incubated with Z-cHOClate for 10 minutes in presence of 100 μM ABAH and were fixed with Methanol at −20°C for 10–15 minutes. This results in permeabilization of plasma membranes as well as phagosomal membranes as indicated by the pH of extracellular and intraphagosomal Z-cHOClate (Supplementary Fig.15a). Cells were then washed and then incubated in 100 mM UB4 buffer containing 140 mM NaCl, 10 mM KCl, 2.5 mM $CaCl_2$ pH 6. HOCl was added (1 nM - 100 μM) and covered with another coverslip immediately. The cells were imaged in the R, B and G channels at t = 0, 2, 3, 6,10, 15 and 20 minutes and R/B values were plotted against each HOCl concentration. The decrease in R/B signal of internalized Z-cHOClate as a function of time quantitatively recapitulates that of extracellular particles upon addition of a known concentration of HOCl to the solution, which also corresponds to the maximum amount of HOCl available in the solution during the experiment i.e, $[HOCl]_{max}$. This that cellular membranes are effectively permeabilized as, the change in probe signal reveals that the levels of extracellular and phagosomal HOCl were comparable (Supplementary Fig. 15b). The initial rate of change of probe signal reflects the rate of HOCl production by MPO and corresponds to a given phagosomal $[HOCl]_{max}$.

We found a 60%-decrease in R/B signal at 20 min that corresponded to ~5 μM of HOCl at pH 6. The decrease in R/B signal observed in Figure 3e of the main manuscript is ~50%, which corresponds to 1–5 μM of HOCl generated endogenously in macrophage phagosomes. The maximal signal decrease observable with Z-cHOClate in 20 minutes is ~95% at pH 6, corresponding to 50–100 μM HOCl. This is also seen with Z-cHOClate in neutrophils (Figure S18c). Cumulatively, this indicates that in macrophage phagosomes the threshold effect is not applicable, and that the maximum concentration of HOCl generated therein is in the order of 1–10 μM.

In cellulo specificity

All inhibitor treatments were performed in DMEM followed by pulsing with Z-cHOClate (~10^4 particles) for 10 minutes in DMEM containing 10% FBS and inhibitor of choice, washed, and imaged in fresh DMEM containing inhibitor for every 10 minutes. All steps prior to imaging were done at 37°C, 5%CO_2. To evaluate *in cellulo* specificity, J774A.1 cells were treated with i) 100 μM ABAH for 3 h for MPO inhibition, ii) 20 μM DPI for 30 minutes for NOX2 inhibition, iii) 200 nM 1400W for 1 h for iNOS inhibition and iv) (20 −100 μM) of NPPB for 1 h for chloride channel inhibition prior to Z- cHOClate pulse[13–16]. Untreated (UT) cells were prepared using the same percentage of DMSO as that of the inhibitor in each case.

In cellulo kinetics

For kinetics experiments J774A.1 cells pretreated with or without 100μM ABAH for 3 hours were used. Cells were pulsed with Z-cHOClate for 5 minutes and used directly for data acquisition (Supplementary Fig. S8a).

Image acquisition

Wide-field images of cell lines and primary cells with Z-cHOClate were acquired using IX83 inverted microscope (Olympus Corporation of the Americas, Center Valley, PA, USA) using a 60X, 1.42 NA, phase contrast oil immersion objective (PLAPON, Olympus Corporation of the Americas, Center Valley, PA, USA) and Evolve Delta 512 EMCCD camera (Photometrics, USA). Filter wheel, shutter and CCD camera were controlled by using MetaMorph software (Molecular Devices, PA). Atto-488 channel images (referred to as 'B') were acquired using 480/20 band pass excitation filter, 535/40 band pass emission filter and 86023bs-FITC/Cy5 as dichroic filter. Cy5 channel images (referred to as 'R') were obtained using 640/30 band pass excitation filter, 690/50 band pass emission filter and HQ665lp- long pass dichroic filter. R6G channel images (referred to as 'G') were obtained using 530/30 band pass excitation filter, 575/40 band pass emission filter and 49014 mKO/mOrange- long pass dichroic filter.

Image analysis

Image analysis was performed using ImageJ software (NIH). All images were subjected to background subtraction using a rolling ball method with a radius of 12 pixels. For kinetics analysis, only Z-cHOClate showing uptake in the DIC channel were considered. For all steady state images, phagosomes of acidic pH ~ 6, i.e., G/B value between 1.5 to 2.5 were considered for HOCl calculations. Data is represented as SEM of three independent replicates.

Statistics

In vitro fluorescence experiments of cHOClate for HOCl sensing, pH sensing and specificity were done in 3 independent replicates on three different days and data is presented as mean and error bars represent SEM for indicated conditions. For *in cellulo* imaging of HOCl and pH we considered 50–100 phagosomes from each imaging dish. Three such experiments, performed on three different days for each experimental condition, i.e., inhibitor used, cell type used etc. The mean and the SEM of these three different experiments was then calculated and plotted.

Immunostaining of Myeloperoxidase (MPO)

Immunostaining was done as described previously[58]. Briefly, Human monocyte derived macrophages (HMDMs) were differentiated on a glass bottom 3.5 cm imaging dish and treated with or without 100 ng/mL LPS for 24 hours. Cells were pulsed with R6G-Z in DMEM with 10% FBS for 15 minutes at 37°C, 5% CO_2, washed with PBS, pH 7.4, and pulsed with DMEM with 10% FBS. The cells were then washed with PBS, pH 7.4, and fixed using 4% paraformaldehyde at RT for 20 mins. Subsequently, cells were permeabilized using 0.25% Triton X-100 and blocked using 3% BSA in PBS. Cells were then incubated

with rabbit polyclonal anti-MPO antibody (Abcam Cat # ab 9535, 1:200 dilution) in blocking buffer for 1 hour at RT (0.3% BSA in PBS). Cells were then washed for 5 minutes with PBS. Goat anti-rabbit secondary antibody conjugated with Alexa Fluor 647 (1:1000 dilution) was added to the cells and incubated for 1h at RT. Cells were washed again to remove excess secondary antibody using PBS for 5 minutes. DAPI (5 μM) was added 10 minutes prior to imaging to stain nuclear DNA in PBS, pH 6. Cell were then imaged on a Leica SP8 laser scanning confocal microscope (Leica Microsystems, Inc., Buffalo Grove, IL) using excitation wavelengths 405 nm (DAPI), 530 nm (R6G) and 650 nm (AlexaFluor 647). Images were processed using Fiji and maximum intensity projected images of Z-planes were presented. For quantification of MPO intensity, mean MPO intensity from 20 cells with or without Zym-R6G was considered.

A similar protocol was followed for mouse bone marrow derived macrophages (BMDMs). J774.1 cells were cultured on a glass bottom 3.5 cm imaging dish to reach 60% confluency, and the same protocol was followed.

Western blot

J774A.1 grown on a 60 mm dish were treated with zymosan particles and allowed to phagocytose for 30 minutes. As control, J774A.1 cells not treated with zymosan were used. Total protein was isolated according to standard procedures and quantified using nanodrop. An aliquot (100 μg) of each lysate was subjected to 8% SDS-PAGE and transferred to nitrocellulose using standard protocol. The nitrocellulose membrane was incubated with a mixture of 1:500 dilution rabbit polyclonal anti-MPO antibody (Abcam Cat # ab 9535) and 1:2000 dilution of mouse monoclonal anti-actin antibody (Abcam Cat # ab 14128) overnight at 4 °C. The membranes were washed and probed with a mixture of 1: 2000 dilution of HRP conjugated goat anti-rabbit antibody (Invitrogen G-21234) and anti-mouse antibody (Invitrogen G-21040) for 1 h at room temperature. The bands for MPO and actin were visualized by chemiluminescence using supersignal for western blot (Thermo Fisher Cat # 80844-07-1).

Integrity of DNA duplex to ROS *in vitro* and *in cellulo*

The integrity of the DNA scaffold comprising cHOClate was evaluated using pcHOClate as a proxy. pcHOClate was formed by annealing IV and V as reported for cHOClate (Supplementary Fig. 6a). Here, EtBr is covalently attached to the 5’ end of V in pcHOClate. EtBr exhibits enhanced fluorescence due to intercalation into the intact duplex DNA of pcHOClate (ϕ_{free}= 0.03,ϕ_{ic} = 0.3). Thus, as long as the duplex is intact, the fluorescence of the intercalated EtBr moiety should not change.

100 nM pcHOClate was incubated with 1–450 μM of NaOCl, or 100 μM of H_2O_2 (in 100 mM UB_4 buffer, pH 7) for up to 30 minutes, which is the maximum duration of our imaging experiments. Spectra of EtBr and **1** were acquired in respective channels and intensities were plotted as functions of HOCl concentration. (Supplementary Fig. 6b, c and d). We observe no change in the intensity of the EtBr over the entire duration in these harsh *in vitro* conditions, indicating the high likelihood of preservation of the duplexed state of cHOClate within the phagosome for the duration of the experiment.

Stability of DNA cHOClate in phagosome was studies using z-pcHOClate. z-pcHOClate was synthesized exactly as reported for Z-cHOClate in the manuscript and characterized by fluorescence microscopy (Supplementary Fig 7 a–b). Z-pcHOClate is has the same DNA duplex, but which bears a covalently attached ethidium bromide (EtBr) dye.

J774A.1 cells were pulsed with Z-pcHOClate for 5 minutes, and images were acquired every 3 minutes for 1 hour in both DIC and EtBr channels. The EtBr intensity of internalized particles was normalized to the intensity of uninternalized particles in the same images and plotted as a function of time. Values at each time point are normalized to the particle intensity at t = 0, (Supplementary Fig 9. c–d). There is undetectable change in EtBr intensity in phagocytosed *Z*-pcHOClate that indicates that the reporter integrity is maintained for ~1 hour in phagosomes. Thus Z-cHOClate is a reliable ratiometric reporter for phagosomal HOCl at least up to ~1 h.

Supplementary Material

Refer to Web version on PubMed Central for supplementary material.

Acknowledgements

We thank Prof V. Rawal and Dr A. Veetil for valuable discussions, A. Hoffman and K. Schoenfelt for providing macrophages, blood donors and K. Becker for help with blood draws, M. Zajac and K. Chakraborty for manuscript editing and the Integrated Light Microscopy facility at the University of Chicago. This work was supported by the University of Chicago Women's Board, Pilot and Feasibility award from an NIDDK center grant P30DK42086 to the University of Chicago Digestive Diseases Research Core Center, R01 DK102960, MRSEC grant no. DMR-1420709, and University of Chicago start-up funds to Y.K. Y.K. is a Brain Research Foundation Fellow.

References

1. Chernyak L & Tauber AI The birth of immunology: Metchnikoff, the embryologist. Cell Immunol 117, 218–233 (1988). [PubMed: 3052859]
2. Robinson JM Reactive oxygen species in phagocytic leukocytes. Histochem Cell Biol 130, 281–297 (2008). [PubMed: 18597105]
3. Winterbourn CC & Kettle AJ Redox reactions and microbial killing in the neutrophil phagosome. Antioxid Redox Signal 18, 642–660 (2013). [PubMed: 22881869]
4. Segal AW How neutrophils kill microbes. Annu Rev Immunol 23, 197–223 (2005). [PubMed: 15771570]
5. Bhavsar AP, Guttman JA & Finlay BB Manipulation of host-cell pathways by bacterial pathogens. Nature 449, 827–834 (2007). [PubMed: 17943119]
6. Klebanoff SJ, Kettle AJ, Rosen H, Winterbourn CC & Nauseef WM Myeloperoxidase: a front-line defender against phagocytosed microorganisms. J Leukoc Biol 93, 185–198 (2013). [PubMed: 23066164]
7. Hampton MB, Kettle AJ & Winterbourn CC Inside the neutrophil phagosome: oxidants, myeloperoxidase, and bacterial killing. Blood 92, 3007–3017 (1998). [PubMed: 9787133]
8. Aratani Y Myeloperoxidase: Its role for host defense, inflammation, and neutrophil function. Arch Biochem Biophys 640, 47–52 (2018). [PubMed: 29336940]
9. Klebanoff SJ Myeloperoxidase: friend and foe. J Leukoc Biol 77, 598–625 (2005). [PubMed: 15689384]
10. Chen JW, Breckwoldt MO, Aikawa E, Chiang G & Weissleder R Myeloperoxidase-targeted imaging of active inflammatory lesions in murine experimental autoimmune encephalomyelitis. Brain 131, 1123–1133 (2008). [PubMed: 18234693]

11. Pulli B. et al. Measuring myeloperoxidase activity in biological samples. PLoS ONE 8, e67976 (2013).
12. Robaszkiewicz A, Bartosz G & Soszynski M. Detection of 3-chlorinated tyrosine residues in human cells by flow cytometry. J Immunol Methods 369, 141–145 (2011). [PubMed: 21620854]
13. Xu Q. et al. A highly specific fluorescent probe for hypochlorous acid and its application in imaging microbe-induced HOCl production. J Am Chem Soc 135, 9944–9949 (2013). [PubMed: 23742029]
14. Shepherd J. et al. A fluorescent probe for the detection of myeloperoxidase activity in atherosclerosis-associated macrophages. Chem Biol 14, 1221–1231 (2007). [PubMed: 18022561]
15. Oushiki D. et al. Development and application of a near-infrared fluorescence probe for oxidative stress based on differential reactivity of linked cyanine dyes. J Am Chem Soc 132, 2795–2801 (2010). [PubMed: 20136129]
16. Lou Z, Li P, Song P & Han K. Ratiometric fluorescence imaging of cellular hypochlorous acid based on heptamethine cyanine dyes. Analyst (Lond) 138, 6291–6295 (2013). [PubMed: 23986031]
17. Sun M. et al. Oxidative cleavage-based near-infrared fluorescent probe for hypochlorous acid detection and myeloperoxidase activity evaluation. Anal Chem 86, 671–677 (2014). [PubMed: 24308562]
18. Kenmoku S, Urano Y, Kojima H & Nagano T. Development of a highly specific rhodamine-based fluorescence probe for hypochlorous acid and its application to real-time imaging of phagocytosis. J Am Chem Soc 129, 7313–7318 (2007). [PubMed: 17506554]
19. Saha S, Prakash V, Halder S, Chakraborty K & Krishnan Y. A pH-independent DNA nanodevice for quantifying chloride transport in organelles of living cells. Nat Nanotechnol 10, 645–651 (2015). [PubMed: 26098226]
20. Modi S. et al. A DNA nanomachine that maps spatial and temporal pH changes inside living cells. Nat Nanotechnol 4, 325–330 (2009). [PubMed: 19421220]
21. Chakraborty K, Leung K & Krishnan Y. High lumenal chloride in the lysosome is critical for lysosome function. elife 6, e28862 (2017).
22. Sharma S, Zaveri A, Visweswariah SS & Krishnan Y. A fluorescent nucleic acid nanodevice quantitatively images elevated cyclic adenosine monophosphate in membrane-bound compartments. Small 10, 4276–4280 (2014). [PubMed: 25044725]
23. Surana S, Bhat JM, Koushika SP & Krishnan Y. An autonomous DNA nanomachine maps spatiotemporal pH changes in a multicellular living organism. Nat Commun 2, 340 (2011). [PubMed: 21654640]
24. Chakraborty K, Veetil AT, Jaffrey SR & Krishnan Y. Nucleic Acid-Based Nanodevices in Biological Imaging. Annu Rev Biochem 85, 349–373 (2016). [PubMed: 27294440]
25. Panchuk-Voloshina N. et al. Alexa Dyes, a Series of New Fluorescent Dyes that Yield Exceptionally Bright, Photostable Conjugates. Journal of Histochemistry & Cytochemistry 47, 1179–1188 (1999). [PubMed: 10449539]
26. Nüsse O. Biochemistry of the phagosome: the challenge to study a transient organelle. ScientificWorldJournal 11, 2364–2381 (2011). [PubMed: 22194668]
27. Yeung T, Touret N & Grinstein S. Quantitative fluorescence microscopy to probe intracellular microenvironments. Curr Opin Microbiol 8, 350–358 (2005). [PubMed: 15939361]
28. King CC, Jefferson MM & Thomas EL Secretion and inactivation of myeloperoxidase by isolated neutrophils. J Leukoc Biol 61, 293–302 (1997). [PubMed: 9060452]
29. Canton J, Khezri R, Glogauer M & Grinstein S. Contrasting phagosome pH regulation and maturation in human M1 and M2 macrophages. Mol Biol Cell 25, 3330–3341 (2014). [PubMed: 25165138]
30. Yuan L, Lin W & Feng Y. A rational approach to tuning the pKa values of rhodamines for living cell fluorescence imaging. Org Biomol Chem 9, 1723–1726 (2011). [PubMed: 21258698]
31. Underhill DM Macrophage recognition of zymosan particles. J Endotoxin Res 9, 176–180 (2003). [PubMed: 12831459]
32. Ohno N. et al. Inflammatory and immunopharmacological activities of metaperiodate oxidized zymosan. Zentralbl Bakteriol 289, 63–77 (1999). [PubMed: 10096168]

33. Zimmerman JF et al. Cellular uptake and dynamics of unlabeled freestanding silicon nanowires. Sci. Adv. 2, e1601039 (2016).
34. Di A. et al. CFTR regulates phagosome acidification in macrophages and alters bactericidal activity. Nat Cell Biol 8, 933–944 (2006). [PubMed: 16921366]
35. Champion JA, Walker A & Mitragotri S. Role of particle size in phagocytosis of polymeric microspheres. Pharm Res 25, 1815–1821 (2008). [PubMed: 18373181]
36. Jiang L. et al. Intracellular chloride channel protein CLIC1 regulates macrophage function through modulation of phagosomal acidification. J Cell Sci 125, 5479–5488 (2012). [PubMed: 22956539]
37. Aiken ML, Painter RG, Zhou Y & Wang G. Chloride transport in functionally active phagosomes isolated from Human neutrophils. Free Radic Biol Med 53, 2308–2317 (2012). [PubMed: 23089227]
38. Hackam DJ et al. Regulation of phagosomal acidification. Journal of Biological Chemistry 272, 29810–29820 (1997). [PubMed: 9368053]
39. Odobasic D, Kitching AR & Holdsworth SR Neutrophil-Mediated Regulation of Innate and Adaptive Immunity: The Role of Myeloperoxidase. J Immunol Res 2016, 2349817 (2016).
40. McMillen TS, Heinecke JW & LeBoeuf RC Expression of human myeloperoxidase by macrophages promotes atherosclerosis in mice. Circulation 111, 2798–2804 (2005). [PubMed: 15911707]
41. Brennan ML et al. Increased atherosclerosis in myeloperoxidase-deficient mice. J Clin Invest 107, 419–430 (2001). [PubMed: 11181641]
42. Morais N. G. de, Costa T. B.da , Almeida T. M. de, Severo MS & Castro C. M. M. B. de. Immunological parameters of macrophages infected by methicillin resistant/sensitive Staphylococcus aureus. J. Bras. Patol. Med. Lab 49, 84–90 (2013).
43. Tlili A, Dupré-Crochet S, Erard M & Nüsse O. Kinetic analysis of phagosomal production of reactive oxygen species. Free Radic Biol Med 50, 438–447 (2011). [PubMed: 21111807]
44. VanderVen BC, Yates RM & Russell DG Intraphagosomal measurement of the magnitude and duration of the oxidative burst. Traffic 10, 372–378 (2009). [PubMed: 19183302]
45. Wong C-O et al. Lysosomal degradation is required for sustained phagocytosis of bacteria by macrophages. Cell Host Microbe 21, 719–730.e6 (2017). [PubMed: 28579255]
46. Chan J, Dodani SC & Chang CJ Reaction-based small-molecule fluorescent probes for chemoselective bioimaging. Nat Chem 4, 973–984 (2012). [PubMed: 23174976]
47. Strzepa A, Pritchard KA & Dittel BN Myeloperoxidase: A new player in autoimmunity. Cell Immunol 317, 1–8 (2017). [PubMed: 28511921]
48. Al-Amran FF & Shahkolahi M. Oxytocin ameliorates the immediate myocardial injury in heart transplant through down regulation of the neutrophil dependent myocardial apoptosis. Heart Views 15, 37–45 (2014). [PubMed: 25104981]
49. Kumar AP & Reynolds WF Statins downregulate myeloperoxidase gene expression in macrophages. Biochem Biophys Res Commun 331, 442–451 (2005). [PubMed: 15850779]
50. Michalski R, Zielonka J, Hardy M, Joseph J & Kalyanaraman B. Hydropropidine: a novel, cell-impermeant fluorogenic probe for detecting extracellular superoxide. Free Radic Biol Med 54, 135–147 (2013). [PubMed: 23051008]
51. Setsukinai K, Urano Y, Kakinuma K, Majima HJ & Nagano T. Development of novel fluorescence probes that can reliably detect reactive oxygen species and distinguish specific species. J Biol Chem 278, 3170–3175 (2003). [PubMed: 12419811]
52. Lin VS, Dickinson BC & Chang CJ Boronate-based fluorescent probes: imaging hydrogen peroxide in living systems. Meth Enzymol 526, 19–43 (2013). [PubMed: 23791092]
53. Robinson KM & Beckman JS Synthesis of peroxynitrite from nitrite and hydrogen peroxide. 396, 207–214 (2005).
54. Abo M. et al. Development of a highly sensitive fluorescence probe for hydrogen peroxide. J Am Chem Soc 133, 10629–10637 (2011). [PubMed: 21692459]
55. Kratz M. et al. Metabolic dysfunction drives a mechanistically distinct proinflammatory phenotype in adipose tissue macrophages. Cell Metab 20, 614– 625 (2014). [PubMed: 25242226]

56. Becker L. et al. Unique proteomic signatures distinguish macrophages and dendritic cells. PLoS ONE 7, e33297 (2012).

57. Zhang X, Goncalves R & Mosser DM The isolation and characterization of murine macrophages. Curr Protoc Immunol **Chapter 14,** Unit 14.1 (2008).**Chapter 14,**

58. Veetil AT, Jani MS & Krishnan Y. Chemical control over membrane-initiated steroid signaling with a DNA nanocapsule. Proc Natl Acad Sci U S A (2018). doi:10.1073/pnas.1712792115

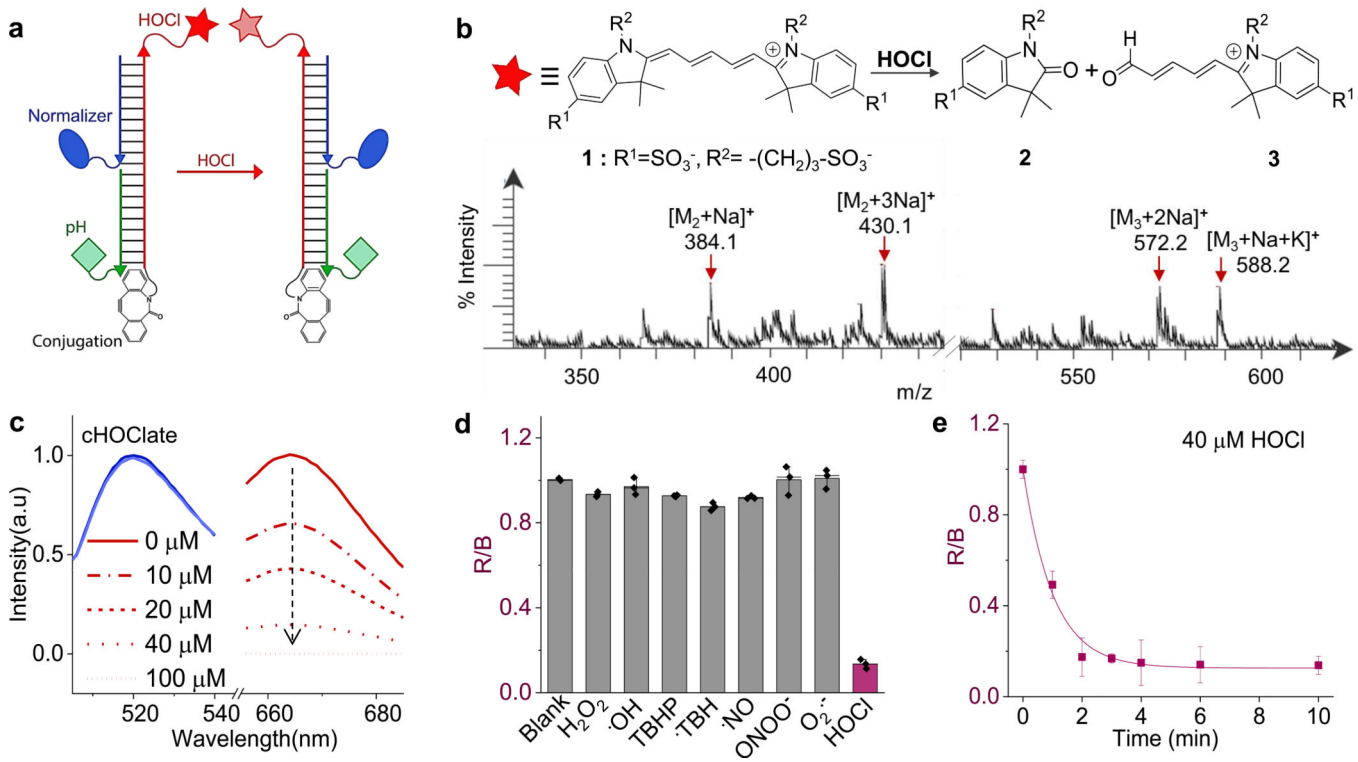

Figure 1. Design of and HOCl sensitivity of cHOClate.

a) Structure and working principle of HOCl sensing by cHOClate. cHOClate comprises a (i) HOCl sensing module (red strand) namely, a HOCl sensitive fluorophore (**1**, red star(R)), (ii) pH sensing module (green strand) namely a pH sensitive fluorophore (R6G, green diamond(G)), (iii) a Normalizer (blue strand) containing a HOCl and pH insensitive fluorophore (Atto-488, blue oval (B)), (iv) a conjugation module, namely a DBCO group at the 5' end of HOCl sensing module. Upon reaction with HOCl **1** undergoes a decrease in fluorescence (1a left). **b**) **1** undergoes oxidative cleavage with HOCl to **2** and **3**. Mass spectral characterization of HOCl cleaved products from **1** (**b** bottom), representative data from two independent experiments are shown. **c)** Normalized fluorescence spectra of cHOClate in R (λ_{ex}=650 nm) and B (λ_{ex}=488 nm) channel with various concentrations of HOCl, pH 4.5, 20mM UB_4 buffer, representative data from three independent experiments are shown. **d)** Sensitivity of *cHOClate* to different ROS or RNS as R/B ratio, pH 4.5, 20mM UB_4 buffer. [HOCl] = 40 μM. all other ROS/RNS donors = 100 μM. **e)** Kinetics of HOCl sensing by cHOClate with 40 μM of HOCl with time, data points were fitted on origin using nonlinear curve fit. Representative data from three independent experiments are shown in **d** and **e**; error bars, SEM; measure of center, mean.

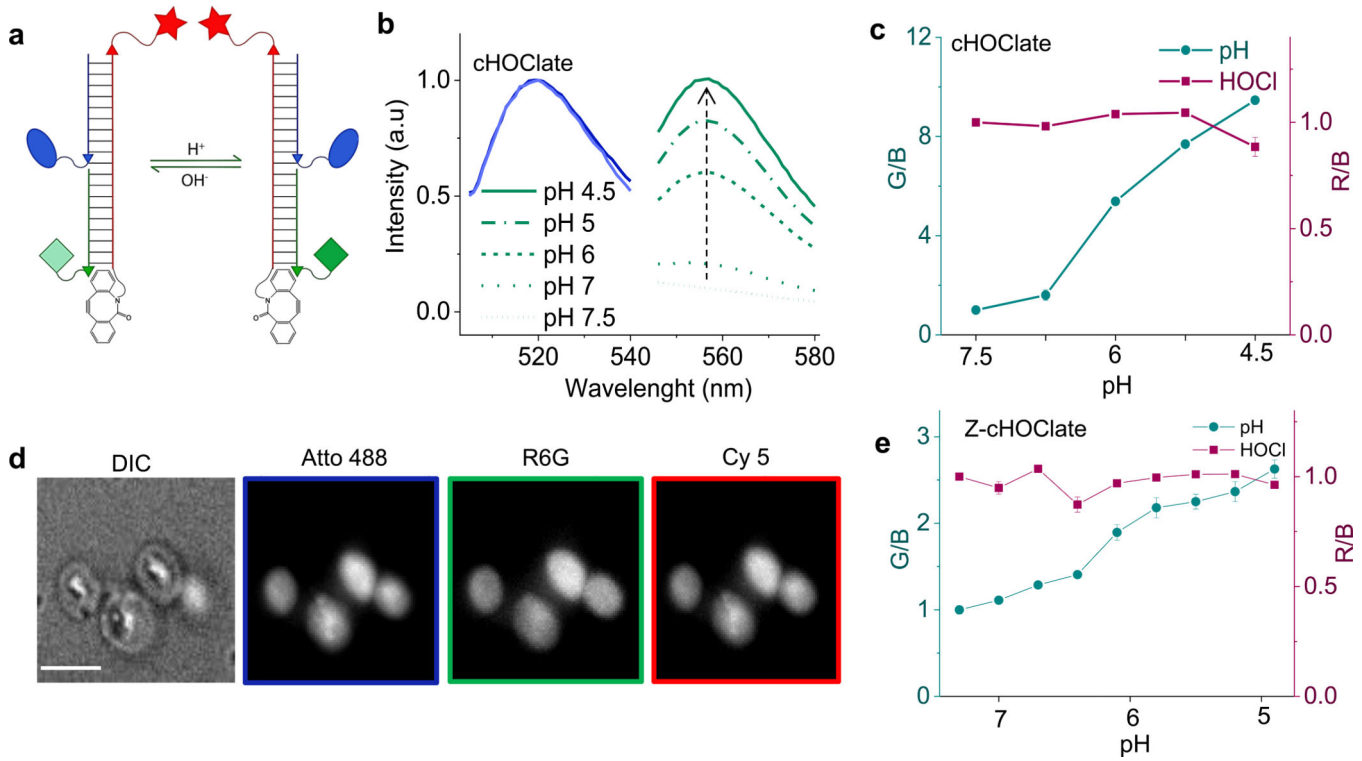

Figure 2. pH sensitivity of cHOClate and Z-cHOClate.

a) pH sensing dye on cHOClate (R6G, green diamond, G undergoes a reversible increase of fluorescence in acidic pH, while R and B remains unaffected. **b)** Normalized fluorescence spectra of cHOClate in B (λ_{ex}=488 nm) and G (λ_{ex}=530 nm) channels with pH, representative data from three independent experiments are shown. **c)** Normalized G/B from and R/B plotted against pH for cHOClate. **d)** Z-cHOClate in DIC, B, G and R channels. Scale bar = 5 μm, representative data from three independent experiments are shown. **e**) Normalized G/B and R/B for Z-cHOClate from pH 7.4 to pH 5, n ≥ 150 particles. Representative data from three independent experiments are shown in **c** and **e**; error bars, SEM; measure of center, mean.

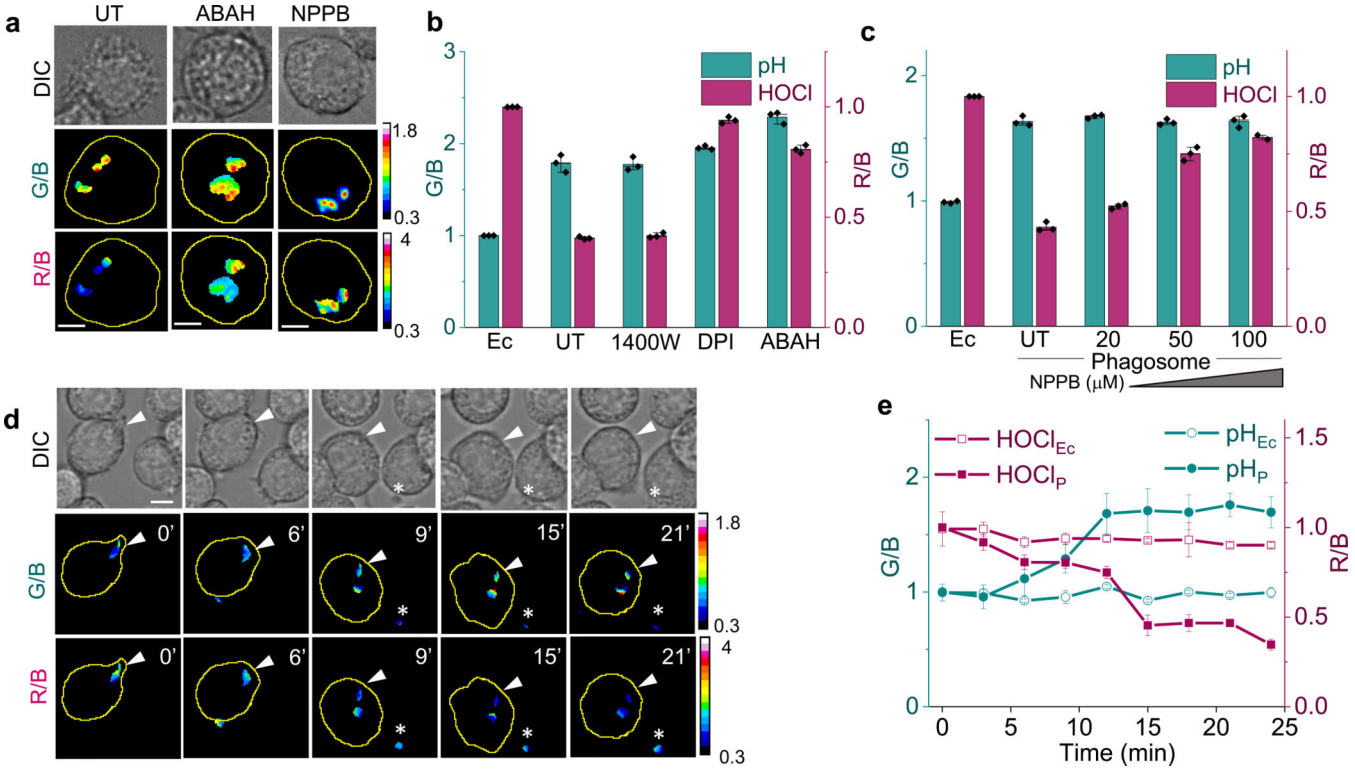

Figure 3. Z-cHOClate senses phagosomal HOCl.

a) Representative images of z-cHOClate in J774A.1 cells at t = 20 minutes post internalization in presence of the indicated pharmacological inhibitors, scale bar = 10 μm, representative data from three independent experiments are shown. **b & c**) G/B and R/B ratios from n ≥ 150 phagosomes imaged as in (**a**) in the presence of the indicated inhibitors. UT= untreated cells Ec = extracellular or uninternalized particles. **d**) Representative images of acidification (G/B) in concert with HOCl production (R/B) reported by Z-cHOClate within the phagosome (white arrowhead) and extracellularly (white asterisk), scale bar = 10 μm, representative data from three independent experiments are shown. **e**) G/B and R/B ratios from n= 50 phagosomes as a function of phagosome maturation. Ec=extracellular or uninternalized particles p= phagocytosed particles. Representative data from three independent experiments are shown in **b**, **c** and **e**; error bars, SEM; measure of center, mean.

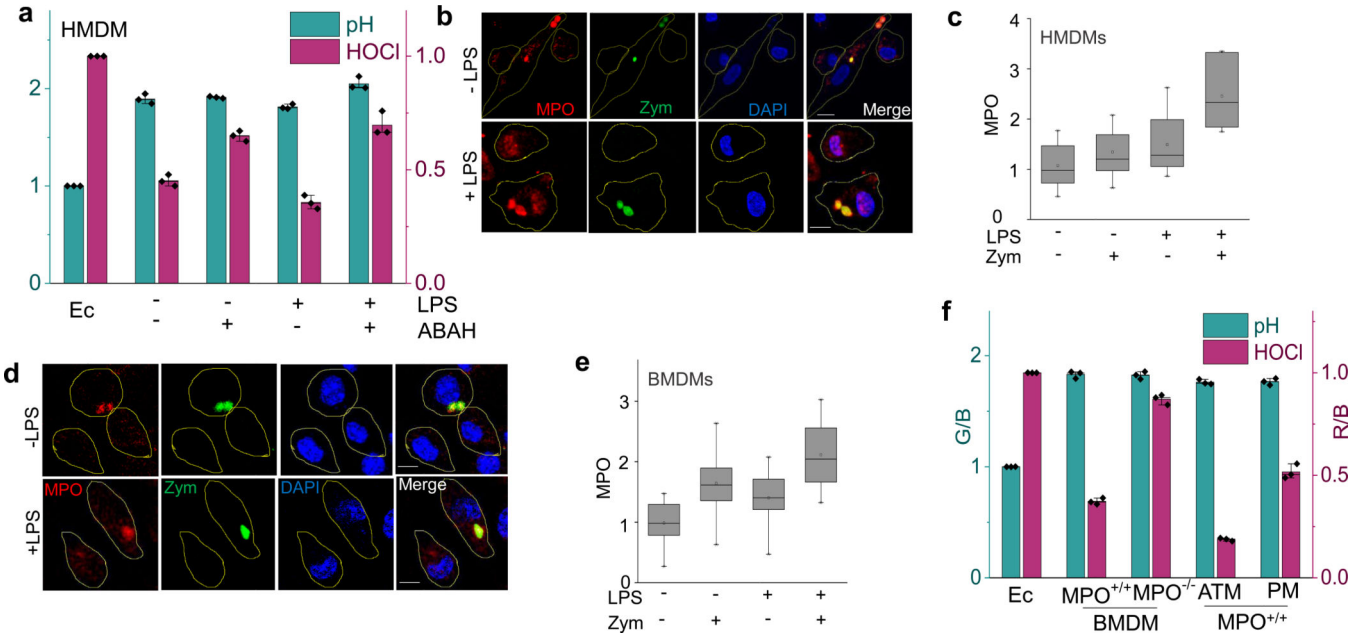

Figure 4. Immunostimulation upregulates MPO in primary macrophages.

a) Phagosomal pH (G/B) and HOCl (R/B) in human monocytes derived macrophages (HMDMs) with or without LPS having phagocytosed z-cHOClate, n ≥ 150 phagosomes. **b)** Immunofluorescence images of MPO (red) in HMDMs with or without LPS treatment and having phagocytosed R_6G-labeled Zymosan (green), scale bar = 10 μm, representative data from three independent experiments are shown. **c)** Mean MPO intensities from (**b**), n = 50 cells. **d)** Immunofluorescence images of MPO (red) in mouse bone marrow derived macrophages (BMDMs) with or without LPS treatment and having phagocytosed R_6G-labeled Zymosan (green), scale bar = 10 μm, representative data from three independent experiments are shown. **e)** Mean MPO intensities from (**d**), n ≥ 50 cells. **f)** Phagosomal pH (G/B) and HOCl (R/B) reported by phagocytosed z-cHOClate in BMDMs derived from $MPO^{+/+}$ and $MPO^{-/-}$ mice, adipose tissue macrophages (ATM) and peritoneal macrophages (PM), n ≥ 150 phagosomes. Representative data from three independent experiments are shown in **a** and **f**; error bars, SEM; measure of center, mean. Box plots in **c** and **e** show a median (center line), mean (open square), upper/lower quartiles (box limits) and maximum/minimum (upper/lower whiskers) from three independent experiments.